# Organization of the Mitotic Chromosome

Natalia Naumova,[1]* Maxim Imakaev,[2]* Geoffrey Fudenberg,[2,3]* Ye Zhan,[1] Bryan R. Lajoie,[1] Leonid A. Mirny,[2]† Job Dekker[1]†

Mitotic chromosomes are among the most recognizable structures in the cell, yet for over a century their internal organization remains largely unsolved. We applied chromosome conformation capture methods, 5C and Hi-C, across the cell cycle and revealed two distinct three-dimensional folding states of the human genome. We show that the highly compartmentalized and cell type–specific organization described previously for nonsynchronous cells is restricted to interphase. In metaphase, we identified a homogenous folding state that is locus-independent, common to all chromosomes, and consistent among cell types, suggesting a general principle of metaphase chromosome organization. Using polymer simulations, we found that metaphase Hi-C data are inconsistent with classic hierarchical models and are instead best described by a linearly organized longitudinally compressed array of consecutive chromatin loops.

The three-dimensional (3D) organization of genomes plays critical roles in regulating chromosomal processes, including gene regulation, DNA replication, and genome stability (*1*–*4*). During the cell cycle, chromosomes transition between two distinct folding states: interphase and metaphase. Interphase chromosomes are relatively decondensed and acquire a cell type–specific spatial organization. In preparation for cell division, chromosomes undergo extensive spatial reorganization and eventually shut down most transcription. This process culminates in a highly condensed and morphologically reproducible metaphase chromosome state.

Chromosome conformation capture (3C)–based methods extend previous characterizations of interphase chromosomes by detecting physical contact frequencies between pairs of genomic loci (*2*, *5*, *6*). During interphase, chromosomes occupy individual territories and are compartmentalized at several hierarchical levels: large multi-megabase active A- and inactive B-compartments (*7*), and smaller sub-megabase topologically associating domains (TADs) (*8*–*10*). At ~100-kb scales, chromatin looping interactions connect genes to distal regulatory elements, mediating long-range gene regulation (*11*).

The internal organization of mitotic chromosomes remains enigmatic (*12*–*15*). On the basis of studies that have used light microscopy, electron microscopy, tomography, and mechanical measurements, several models of mitotic chromosomes have been proposed. These models can be subdivided into three groups (*16*, *17*): loops-on-a-scaffold models (*15*, *18*, *19*), hierarchical models of increasingly thicker coiled or looped fibers (*20*, *21*), and network models, which describe mitotic chromosomes as highly cross-linked

[1]Program in Systems Biology, Department of Biochemistry and Molecular Pharmacology, University of Massachusetts Medical School (UMMS), 368 Plantation Street, Worcester, MA 01605–0103, USA. [2]Institute for Medical Engineering and Science, and Department of Physics, Massachusetts Institute of Technology (MIT), Cambridge, MA 02139, USA. [3]Program in Biophysics, Harvard University, Boston, MA 02115, USA.

*These authors contributed equally to this work.
†Corresponding author. E-mail: job.dekker@umassmed.edu (J.D.); leonid@mit.edu (L.A.M.)

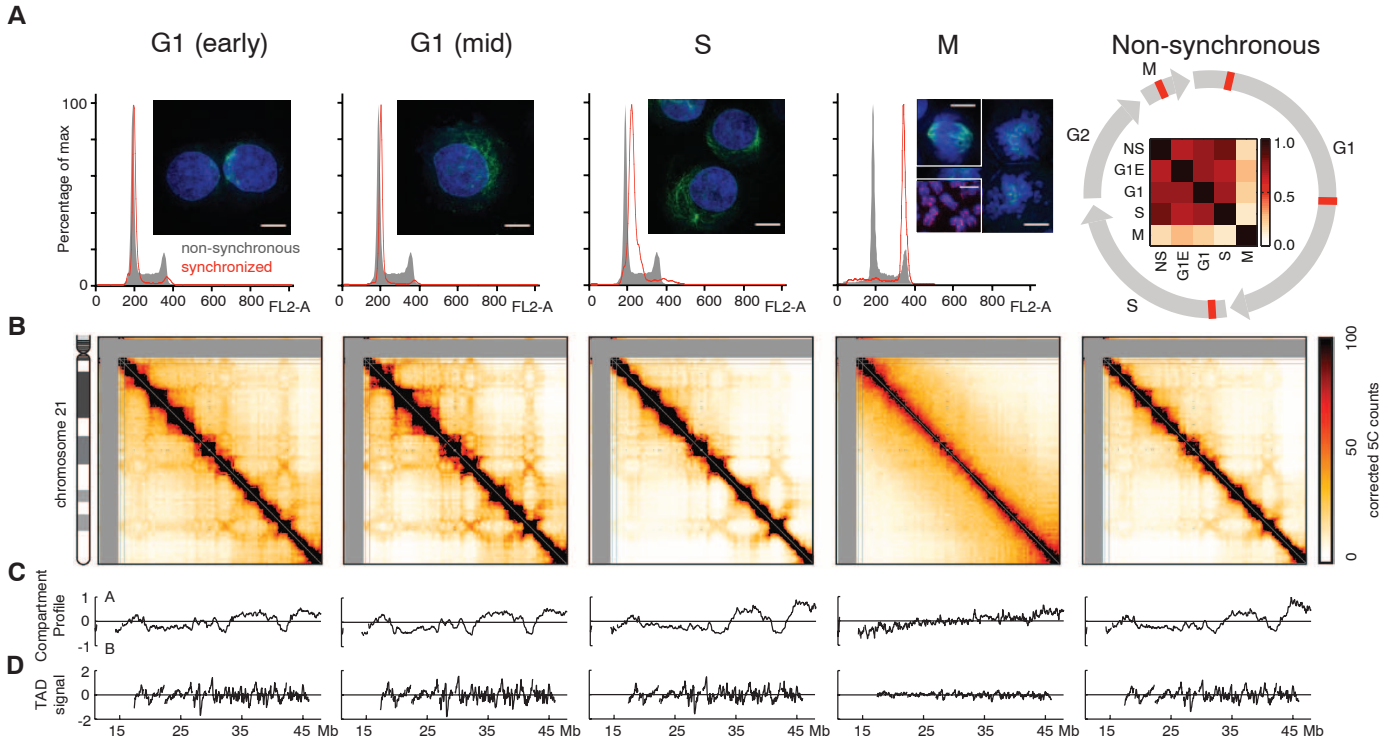


**Fig. 1. Organization of chromosome 21 through the cell cycle.** (**A**) Fluorescence-activated cell sorting profiles and microscopy images of cell populations analyzed in this study. Images show 4′,6-diamidino-2-phenylindole–stained DNA (blue) and α-tubulin (green). Scale bars, 1 μm. Image under "M" shows three different pictures: right half, cells arrested in metaphase (12 hours nocodazole); top left inset, control metaphase cells with intact spindle; bottom left inset, nocodazole-arrested chromosomes stained for SMC2, showing separated sister chromatid arms. (Right) Nonsynchronous population consists of a mixture of all cell-cycle phases. Circular diagram shows cell cycle, with red markers indicating cell-cycle phase of studied synchronization samples. Inside the cell-cycle circle is a correlation matrix between 5C interaction patterns of both nonsynchronous cells and all studied stages of the cell cycle (*27*). (**B**) Corrected 5C matrices of chromosome 21 for these cell populations; raw 5C data were binned to 250 kb with a 50-kb sliding window and corrected by using ICE. Gray regions are not interrogated in this study. (**C**) A/B compartment profile for each data set. (**D**) TAD signal for each data set.

gels (*22*, *23*), as well as models that combine these different features (*24*).

We applied chromosome conformation capture carbon copy (5C) (*25*) and Hi-C (*7*) to study the spatial organization of human chromosomes during the cell cycle, revealing two distinct folding states. Using polymer simulations, we evaluated existing and new models of metaphase chromosome organization. We propose that metaphase organization can emerge through a two-stage process: linear compaction by consecutive chromatin loops, potentially generated by structural maintenance of chromosomes (SMC) complexes, followed by axial compression.

## Results

### *Changes in Chromosome Organization During the Cell Cycle*

For our initial studies, we used HeLa S3 cells because large and homogeneous populations of these cells at various stages of the cell cycle can be obtained relatively easily and efficiently (fig. S1). The HeLa S3 karyotype is complex, but stable. We focused analyses on intra-chromosomal data from six chromosomes that appear normal, as judged by use of spectral karyotyping/multiplex fluorescence in situ hybridization (SKY/M-FISH) and Hi-C (figs. S2 and S3). Further, our analyses use ICE (iterative correction and eigenvector decomposition) (*26*), which corrects for biases in sequencing coverage that may arise from copy-number alterations.

We used 5C technology to study the organization of small and un-rearranged chromosome 21 at different time points throughout the cell cycle (Fig. 1). We interrogated long-range interactions using a pool of 5C primers that cover the length of chromosome 21 with an average spacing of 25 kb (*27*). We studied early-$G_1$ and mid-$G_1$ cells, thymidine-arrested early S-phase cells, and nocodazole-arrested prometaphase ("mitotic") cultures (Fig. 1 and figs. S1 and S4) (*27*). We found that nocodazole treatment up to 12 hours leads to some gradual shortening of mitotic chromosomes, but Hi-C analyses for 3, 7, and 12 hours of incubation yield overall very similar results (fig. S5). Sister chromatid arms are separate and no longer intertwined in nocodazole-arrested cells (Fig. 1A).

The interaction patterns for early-$G_1$, mid-$G_1$, and S-phase are highly correlated with each other and with the pattern obtained with nonsynchronous cells [Spearman correlation coefficient ($r$) > 0.67, $P << 10^{-10}$] (Fig. 1A) (*27*). For these cell-cycle phases, the interaction maps display similar plaid patterns of regional enrichment or depletion of long-range interactions (Fig. 1). A similar plaid pattern was previously observed for nonsynchronous cells, which are mainly (97%) in interphase, and has been interpreted to reflect spatial separation of chromosomes in A/B compartments (*7*).

In mitotic cells, however, the interaction map changes dramatically, and the plaid pattern disappears. The mitotic interaction pattern displays a low correlation with those for all other cell-cycle phases (Spearman $r < 0.27$, $P << 10^{-10}$) (Fig. 1B). Thus, we identify two distinct chromosome folding states in the cell cycle.

### *Loss of Chromosome Compartments and TADs in Metaphase*

Next, we used Hi-C (*7*) to perform a genome-wide analysis of the mitotic and mid-$G_1$ states because these represent the two most distinct states of the cell cycle (Fig. 2 and fig. S6). We then used both 5C and Hi-C data to study features of chromosome organization at different levels: compartments at the chromosome scale, and TADs at the sub-megabase scale. Using ICE (*26*), we obtained compartment profiles. In $G_1$, an alternating compartment profile (Fig. 2B) and preferential

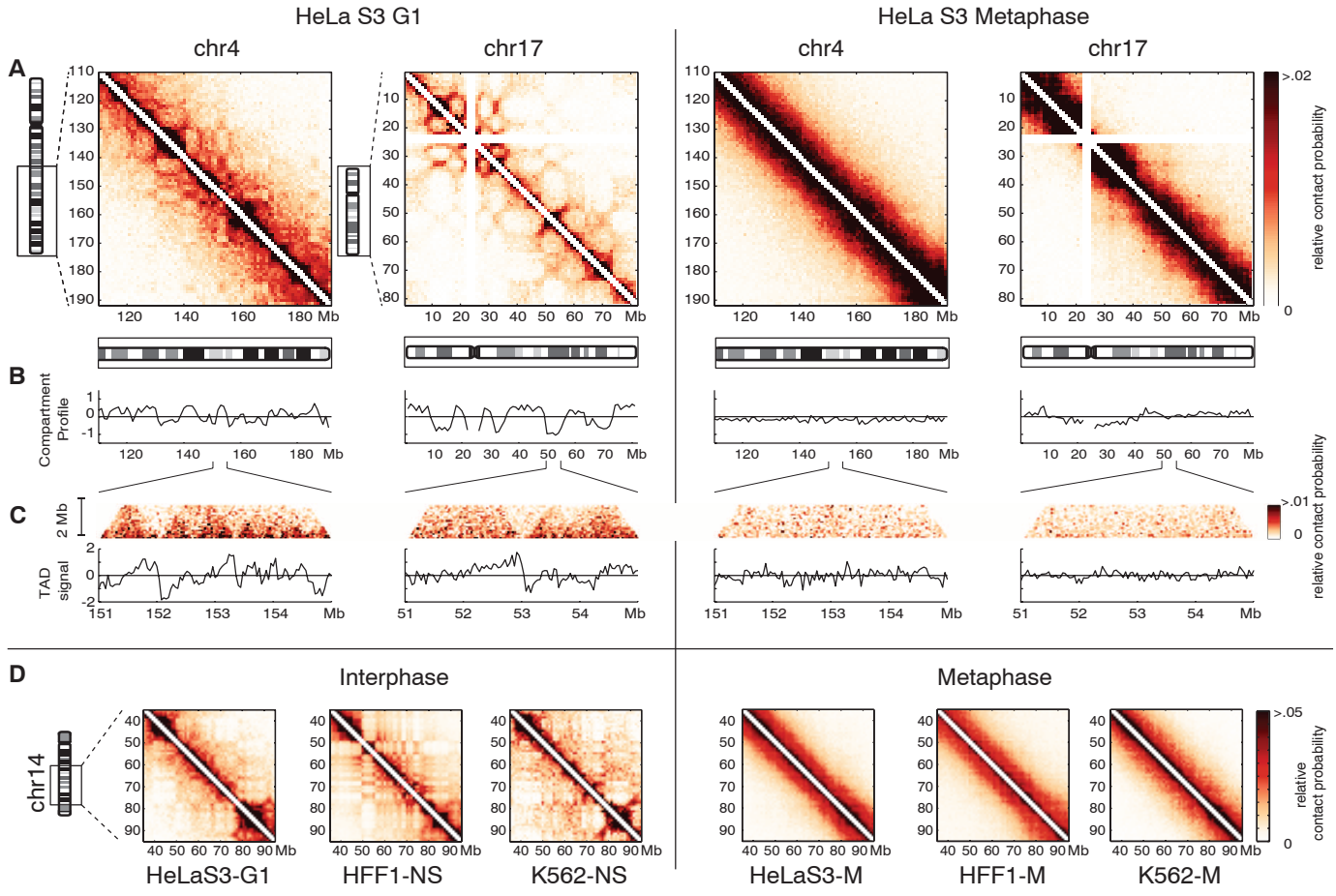


**Fig. 2. Hi-C analysis of chromosome organization in $G_1$ and mitotic cells.** (**A**) Relative Hi-C contact probability maps for chromosome 17 and an equally sized 82-Mb region of chromosome 4, at 1-Mb resolution. M-phase arrest was at 12 hours of nocodazole. (**B**) A/B compartment profile for these regions. (**C**) Zoom-in of 4-Mb subregions. (Top) Region of a contact map at 40-kb resolution. (Bottom) TAD signal for this region. (**D**) Hi-C contact probability maps for a region of chr14 in interphase and metaphase. Displayed are HeLa-S3-$G_1$, HFF1-NS (nonsynchronous), and published K562-NS (*7*) data sets (left) and HeLa-S3-M, HFF1-M, and K562-M data sets (right).

interactions among regions within the same compartment type (fig. S7) were observed, which is in agreement with previous studies on nonsynchronized cells (*7*, *28*). Compartment profiles extracted from 5C agree with Hi-C on chromosome 21 (fig. S8) and are highly correlated in early $G_1$, mid $G_1$, and S-phase cells (Spearman $r > 0.85$, $P << 10^{-10}$).

In mitotic cells, Hi-C interaction maps are very similar for all chromosomes, and compartmentalization disappears across the genome (Figs. 1 and 2) because eigenvector decomposition does not detect a compartment profile that alternates along the length of a chromosomal arm. Consistently, preferential interactions between compartments extracted from $G_1$ Hi-C data, or between regions with similar GC content or similar interphase chromatin marks, are lost in mitosis (fig. S7).

At a sub-megabase scale, chromosomes have been found to be composed of TADs (*9*, *10*). A TAD is a contiguous chromosomal region that largely interacts with itself and is relatively insulated from its direct genomic neighbors. TADs have been identified by their pattern of preferential upstream or downstream interactions: largely downstream at the start of a TAD, and largely upstream at the end (*9*). We quantify the TAD signal by the log2-ratio of upstream to downstream interactions of each genomic region. In interphase, the TAD signal is prominent along all chromosomes (Figs. 1 and 2C), which is consistent between Hi-C and 5C on chromosome 21 ($r = 0.73$, $P < 10^{-10}$) and is more prominent in mid-$G_1$ cells than in early $G_1$ and S phases.

In mitotic cells, the amplitude of the TAD signal is strongly reduced across all chromosomes; this was confirmed by means of 5C on chromosome 21. The residual variation in the TAD signal in mitotic cells can be explained by the presence of around 15% nonmitotic cells in nocodazole-arrested cultures (fig. S9). A high-synchrony (98%) mitotic data set displays further loss of TADs (fig. S10). Hi-C when performed at fourfold lower formaldehyde concentration (0.25%) showed similar results, indicating that loss of compartments and TADs is not due to over–cross-linking of condensed chromosomes (figs. S11 and S12). We conclude that large-scale compartments and sub-megabase TADs are mostly lost in metaphase.

We repeated the analysis of interphase and metaphase chromosome conformation in two additional cell types: erythroid K562 cells and primary human foreskin fibroblasts (HFF1) (Fig. 2D and figs. S13 and S14). In interphase, all three cell types display A/B compartments, but their locations are different (fig. S15). In contrast, the Hi-C data for mitotic chromosomes are strikingly similar for all three cell types, showing loss of compartments and TADs, leading to virtually identical homogeneous interaction maps for all chromosomes. Thus, during the cell cycle chromosomes alternate between cell type–specific and locus-specific interphase organizations and a universal cell-type and locus invariant mitotic conformation.

### *Two Levels of Organization of Mitotic Chromosomes*

Because chromosomes can be understood as long polymers, we examined how the contact probability $P(s)$ derived from Hi-C maps depends on genomic distance, $s$, between a pair of loci in each chromosomal arm (Fig. 3). This dependence is informative of the underlying polymer state (*29*–*31*). $P(s)$ for interphase and mitotic chromosomes are strikingly different while being highly consistent among cell types (Fig. 3A). In contrast to interphase, mitotic chromosomes display a slow decrease in contact probability $P(s) \sim s^{-0.5}$ from 100 kb to 10 Mb, followed by a rapid fall-off at ~10 Mb. These features are observed for all chromosomes irrespective of their lengths (Fig. 3B) and are robust to details of a Hi-C experiment and methods used to compute $P(s)$ (fig. S16).

The two regimes in metaphase $P(s)$ suggest that chromatin is organized differently above and below 10 Mb. Regions separated by more than 10 Mb rarely contact each other and thus occupy distinct spatial positions; this is consistent with the known linear organization of mitotic chromosomes, in which consecutive regions occupy consecutive longitudinal positions. In contrast, loci within any continuous 10-Mb region frequently contact each other. Thus, mitotic chromosomes can be considered as a linearly ordered structure above 10 Mb consisting of spatially mixed layers of ~10 Mb (Fig. 3B).

To understand mitotic chromosome organization within a 10-Mb layer, we compared the observed $P(s)$ with that of the equilibrium globule and fractal globule polymer states. A fractal globule state has $P(s) \sim s^{-1}$ and is characterized by spatial segregation of different regions (Fig. 3C). Conversely, the equilibrium globule state exhibits a plateau in $P(s)$ [$P(s) \sim s^{0}$] and is characterized by a high degree of mixing between different regions of the polymer. The observed $P(s) \sim s^{-0.5}$ in metaphase falls in between $P(s)$ for these two states, indicating an intermediate level of spatial mixing. Thus, although previous work found that a fractal globule state was consistent with interphase $P(s)$ from 500 kb to 7 Mb (*7*), a different polymer model is needed to account for the greatly different $P(s)$ for mitotic chromosomes.

### *Polymer Modeling of Mitotic Chromosome Organization*

We next developed and tested polymer models of the final folded state of a mitotic chromosome. Because details of the folding pathway and initial conformations are unknown, we studied equilibrium polymer models (*27*). For each model, we generated an ensemble of conformations, simulated Hi-C experiments of this ensemble, and evaluated its ability to reproduce the main features of the Hi-C data: the observed $P(s)$ (Fig. 3B) and a homogeneous ensemble-average interaction map (Figs. 1 and 2 and fig. S17). We additionally required that models have the known cylindrical chromosome geometry, chromatin-packing density [~70 Mb per 1 μm of chromatid (*32*)], and linear organization of mitotic chromatids (*33*). We modeled 77 Mb of chromatin



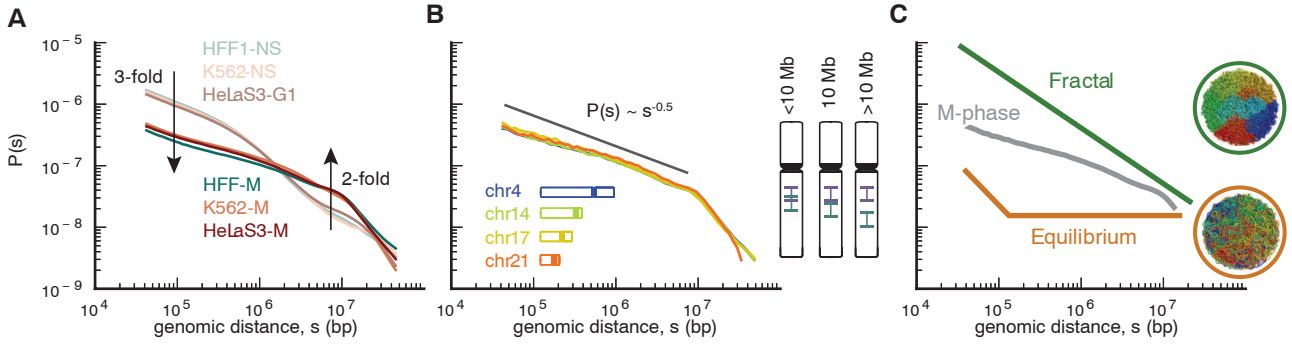


**Fig. 3. Contact probability as a function of genomic distance.** To compare experiments with different numbers of reads, here and below all $P(s)$ plots are normalized to integrate to one. (**A**) Contact probability for interphase and mitotic cells averaged over all chromosomes; data sets are as in Fig. 2D. Arrows indicate fold-change from interphase to metaphase. (**B**) Contact probability for individual HeLa S3 mitotic chromosomes, compared with $P(s) \sim s^{-0.5}$. Diagrams on the right illustrate that loci separated by fewer than 10 Mb occupy overlapping longitudinal positions, whereas loci separated by more than 10 Mb rarely overlap. (**C**) Mitotic $P(s)$ below 10 Mb plotted against schematic $P(s)$ for fractal and equilibrium globule states. Insets show spatial organization of simulated polymer fibers for each state, in which fibers (here and below) are colored from blue to red along their lengths. Observed $P(s)$ for mitotic chromosomes falls in between that of an equilibrium globule, in which regions of the polymer are highly mixed, and a fractal globule, in which different regions are spatially segregated.

(approximately equivalent to chromosome 17, which is 1 μm long and 0.5 μm in diameter) as a polymer of 128,000 monomers, each representing three nucleosomes (~600 bp), with a diameter of 10 nm and a persistence length of 4 monomers (10 to 12 nucleosomes) (*34*). We chose these parameters to best represent a 10-nm fiber (*27*) because the pervasiveness of the 30-nm fiber in vivo has become increasingly contested (*22*, *35*, *36*). Further simulations have shown that our main results hold for a 30-nm fiber, as well as for a more flexible 10-nm fiber (fig. S18), and our results are relatively insensitive to the local structure of the chromatin fiber. Polymer models were simulated by using Langevin dynamics, with interactions and constraints specific to each model. We account for topoisomerase II activity (*37*, *38*) by allowing chromatin fibers to occasionally pass through each other and thus change the topological state of a chromosome (*27*, *39*); this was accomplished by setting a finite energy cost for two monomers to occupy the same volume.

First, we tested whether an equilibrium model with a combination of cylindrical geometry and linear organization is sufficient to reproduce the observed $P(s)$ (Fig. 4A and fig. S19). This model imposes linear organization by constraining monomers to have reproducible mean longitudinal positions with a 120-nm standard deviation (SD) along the longitudinal axis of the chromosome, as observed with microscopy (*33*). Simulations of this model generate a layered chromosome conformation in which the fall-off in contact probability $P(s)$ naturally emerges at ~10 Mb, demonstrating that linear organization and a fall-off in contact probability are connected (fig. S19 and movie S1). However, in contrast to the Hi-C data, models constrained only by cylindrical geometry and linear organization produce $P(s)$ with a plateau from 200 kb to 10 Mb (Fig. 4A) and are highly mixed within a layer, similar to an equilibrium globule (Fig. 3C and fig. S20).

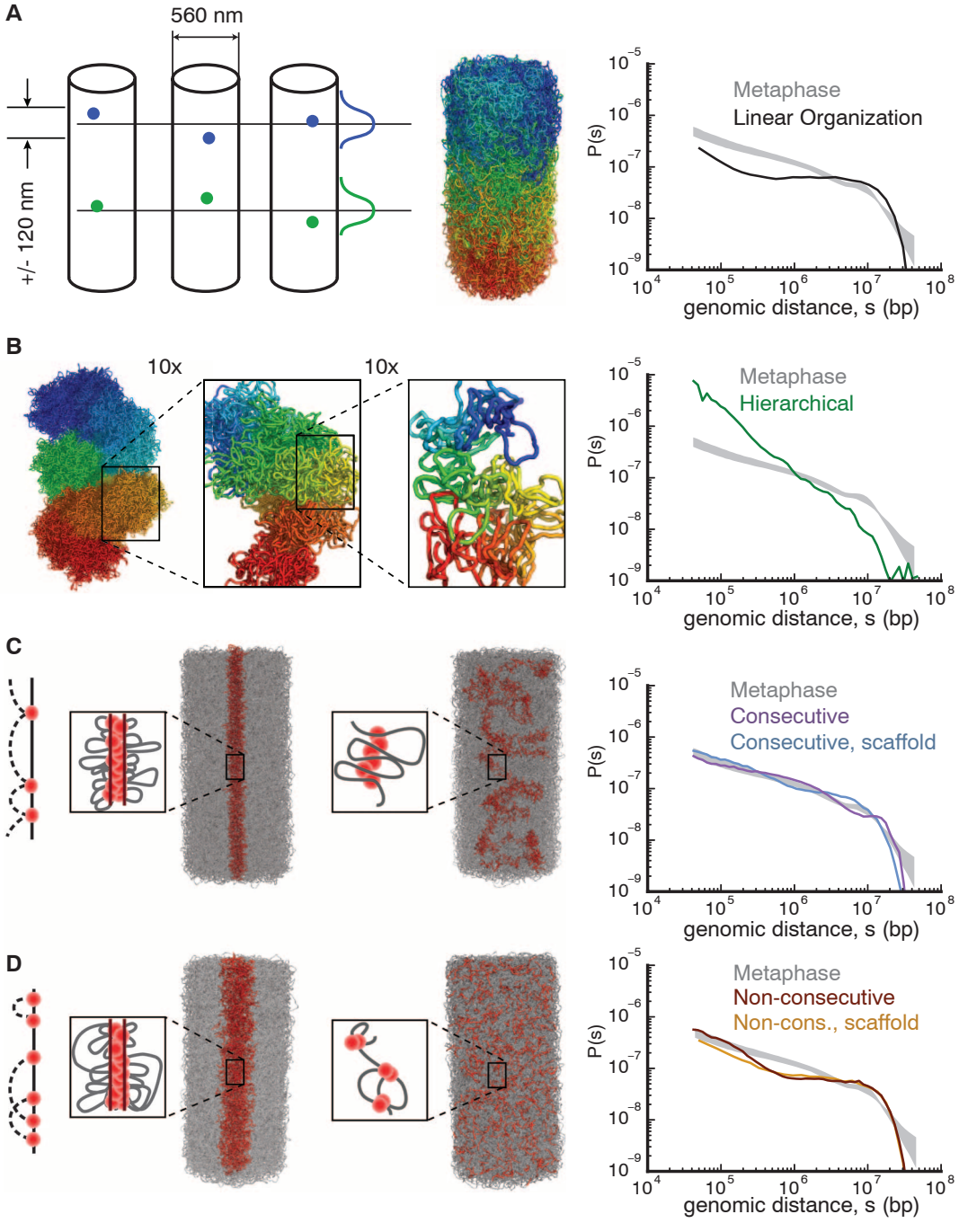


**Fig. 4. Polymer models of mitotic chromosome organization (left) and their corresponding *P*(*s*) (right).** Experimental $P(s)$ in metaphase (gray shaded area) is bounded by minimum and maximum $P(s)$ calculated from six independent Hi-C data sets (three cell lines). (**A**) Linear organization model. Each monomer is constrained to have reproducible mean longitudinal positions with 120 nm SD (illustrated in the diagram, next to an example of a polymer conformation for this model). (**B**) Hierarchical model formed by successively folding the fiber into a next-level fiber, here by using loops with average length of 9 kb, 240 kb, and 4.8 Mb; conformation is colored from blue to red at each level of magnification (figs. S21 and S22). (**C**) Models with consecutive loops, cylindrical geometry, and linear organization. Bases of the loops (red) are either attracted to a central scaffold (left) or free (middle). For optimal loop sizes, $P(s)$ curves for these models approach experimental $P(s)$. (**D**) Models with nonconsecutive loops, cylindrical geometry, and linear organization, either attracted to a central scaffold (left) or free (middle). Nonconsecutive loops are obtained by randomizing positions of consecutive loop bases while maintaining loop lengths. Models with nonconsecutive loops have worse agreement with metaphase $P(s)$ than that of models with consecutive loops (fig. S24).

We evaluated two major classes of models for mitotic chromosomes: hierarchical models (*20*, *21*) and loops/scaffold models (*15*, *18*, *19*). In hierarchical models, the chromatin fiber is successively folded into a thicker fiber at each hierarchical level. Models with both looping and solenoidal twisting at each level were implemented by use of constraints on distances and angles between subsets of monomers (Fig. 4B and figs. S21 and S22). We found that although hierarchical folding can produce chromosomes with the correct geometry and linear organization, the contact probability for these models decreased much more sharply than was observed in Hi-C (Fig. 4B and fig. S22). This indicates that hierarchical models overly constrain the chromatin fiber because most of the contacts occur locally, within the first- and second-level fibers.

To study models with loops emanating from a scaffold (*17*, *18*), we induced formation of consecutive loops, attracted their bases to a central scaffold, and imposed linear ordering and cylindrical geometry (Fig. 4C and movie S2). To form consecutive loops, we chose a random subset of genomic positions as loop bases; each loop base was then connected by harmonic bonds to immediately preceding and subsequent loop bases along the chromosome (*27*). This process forms an array of consecutive nonoverlapping loops with an exponential distribution of loop lengths. For each average loop length, we equilibrated the system (fig. S23) and found that chromosome models with 80 kb average loop size closely reproduce experimental $P(s)$ (Fig. 4C and fig. S18) and yield moderately mixed chromatin organization within layers (fig. S20 and movies S3 and S4). Surprisingly, a scaffold-free model with consecutive 120-kb loops still achieved good agreement with experimental $P(s)$ (Fig. 4C and fig. S18). This stems from the spatial proximity of neighboring consecutive loops and explains how short-range interactions (~100 kb) can increase contact probabilities over much longer ranges (~5 Mb) (fig. S24). Loop sizes for our best-fitting models closely agree with earlier measurements: 80 kb (*40*), 30 to 90 kb (*18*), and 83 ± 29 kb (*41*).

Models with only attraction to a scaffold (fig. S19), or with nonconsecutive loops (Fig. 4D), are inconsistent with experimental $P(s)$. Additionally, cell-to-cell variability in loop positions and sizes is required to reproduce the homogenous population-averaged Hi-C maps (fig. S17). Taken together, stochastic arrays of consecutive loops, either on or off the scaffold, are essential for agreement with Hi-C data.

### *A Two-Step Process for Mitotic Chromosome Folding*

In our polymer models, mitotic chromosome organization is described by two main features: arrays of consecutive 80- to 120-kb loops and linear ordering of loci separated by more than 10 Mb. Consecutive loops could be formed by linear compaction of the chromatin fiber (*42*) by loop-extruding, SMC-containing complexes in early prophase—for example, as proposed by Alipour and Marko (*43*). Arrays of loops have also been proposed for mitotic and meiotic chromosome organization on the basis of cytological and molecular considerations (*44*). Chromosomes with consecutive loops resemble a polymer bottlebrush model (Fig. 5 and fig. S24), which has previously been suggested as a model for condensed chromosomes (*34*). The second feature, linear ordering above 10 Mb, was imposed in our consecutive-loop models of the final folded state (Fig. 4C) but could emerge naturally from axial compression of long prophase chromosomes (*19*, *38*, *42*, *44*). Compression cannot be accomplished by increased chromatin-chromatin affinity alone because this would lead to condensation into a globular geometry (*17*, *34*, *43*). However, mechanisms that locally compress the backbone formed by loop bases naturally allow for active anisotropic compression into a shorter and thicker chromosome, with the same width regardless of chromosome length (*14*). Additionally, differences in the duration or efficiency of the first and second stages of chromosomal condensation provide a natural mechanism for condensation-related proteins to separately affect mitotic chromosome length and width (*23*).

These considerations led us to propose a model in which mitotic chromosomes are formed by a two-stage process (Fig. 5): First, an interphase chromosome is linearly compacted into an array of consecutive loops, forming a prophaselike chromatid of ~5 μm in length and ~1 μm in di-

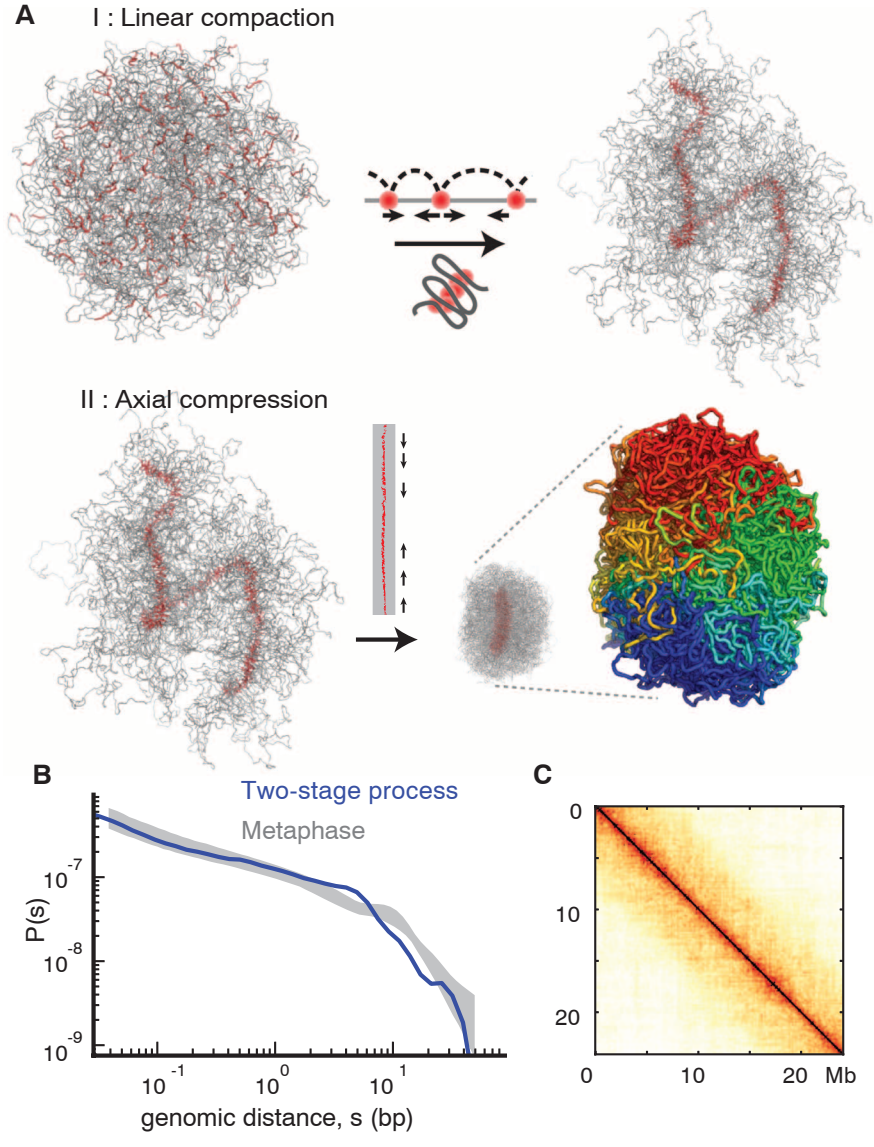


**Fig. 5. A two-stage process of mitotic chromosome folding.** (**A**). Stage I: Linear compaction by formation of consecutive chromosomal loops leads to the formation of a fiber of loop bases. Stage II: Homogeneous axial compression of the fiber's backbone leads to the formation of a dense chromosome. This two-stage process produces a chromosome with the appropriate cylindrical geometry and linear organization (genomic position is indicated by the coloring from blue to red). (**B**) Contact probability $P(s)$ for the two-stage process compared with observed $P(s)$ (gray shaded area, as in Fig. 4). (**C**). Average contact map for chromosomes folded by the two-stage process.

ameter. Second, this chromatid undergoes homogeneous axial compression (*27*).

We simulated the first state by creating an array of consecutive loops, without explicitly modeling loop extrusion. To simulate the second stage, we imposed interactions between nearby loop bases and concomitantly condensed loops using poor solvent conditions. The resulting conformations naturally acquire cylindrical chromosomal geometry and linear ordering and demonstrate good agreement with experimental Hi-C and microscopy data (Fig. 5, fig. S20, and movies S5 and S6).

## Discussion

The interphase and mitotic states represent two functionally distinct 3D organizations of the genome. We found that mitotic chromosomes preserve few if any of the structural features that define interphase chromosomes. We also found that metaphase chromosomes acquire a similar organization in different cell types. This raises the question of how epigenetic information is inherited through mitosis, when transcription largely ceases and many proteins, including RNA polymerase, dissociate from chromosomes. Current models of epigenetic memory involve retention of key transcription factors and chromatin architectural proteins at specific loci ["bookmarking" (*45*)], but roles of higher-order chromatin folding have also been proposed (*46*). In mitotic chromosomes, we not only found that the large-scale spatial segregation into cell type–specific A/B compartments is lost, but that locally folded TADs that are conserved between cell types are also largely absent. Additionally, the homogeneous mitotic interaction maps show no evidence for the emergence of new compartments, including a lack of preferential interactions within chromosomal bands. These observations imply that higher-order chromatin structures have to form de novo in early $G_1$ and do not themselves carry epigenetic memory. It is possible that their reemergence in early $G_1$ is driven by histone marks, DNA methylation, and protein complexes that remain on DNA through mitosis, such as at TAD boundaries (*47*) or at key gene regulatory elements (*48*).

Our proposed model of a metaphase chromosome as a compressed array of consecutive loops (Fig. 4C) is supported by several previously described structural features. Imaging studies have shown that individual loci do not occupy reproducible radial positions (*33*). Additionally, contiguous chromosomal regions of <1 Mb do not fill a full radial cross-section of the chromosome, whereas regions of several megabase do (*49*). Reproduced by our model, these features are consistent with incomplete mixing within a 10-Mb layer (fig. S20). Average loop lengths of 80 to 120 kb, which best reproduce experimental $P(s)$ in our models, agree with previous estimations of loop lengths (*18*, *40*, *41*). We remain agnostic about the role of a scaffold because models with compact, diffuse, or no scaffold agree equally well with Hi-C data (fig. S26). Further, the loops in our models are irregular and would form a uniform density "melt," which is consistent with recent electron microscopy and small-angle x-ray scattering studies (fig. S20) (*22*, *50*).

One aspect makes our proposed model of the mitotic chromosome different from earlier proposals. Several classical models assumed a highly structured folding, with regular solenoids, loops of fixed length, or distinct hierarchical levels. Our model achieves agreement with earlier experiments and our Hi-C data by incorporating variability at all levels of assembly: cell-to-cell differences in loop positions and lengths and substantial mixing within a 10-Mb layer. Moreover, classical models of solenoidal and hierarchical folding would require machinery able to manipulate chromatin at the micrometer and multi-megabase scales; similarly, a recently proposed polymer model (*51*) implies a mechanism to control the formation of long-range loops. Our model, on the contrary, proposes largely local loop formation followed by a linear compression of the resulting backbone of loop bases, allowing the rest of the chromatin fiber to stay in a largely disordered ensemble. The use of local folding mechanisms and the lack of strict sequence-driven control makes this two-stage folding mechanism robust with respect to chromosome sizes, compositions, and genomic rearrangements. However, the current resolution of our data does not rule out the use of different subsets from a large set of specific sequence elements as loop bases in different cells.

Future studies performed at higher resolution—for example, through deeper sequencing of Hi-C libraries, single-cell Hi-C, and at multiple time points through prophase and telophase-early $G_1$—may lead to insights into the finer-scale organization of chromosomes and the intricate folding pathways that connect interphase and mitotic chromosome structures.

### References and Notes


1. J. Dekker, *Science* **319**, 1793–1794 (2008).
2. P. Fraser, W. Bickmore, *Nature* **447**, 413–417 (2007).
3. G. Fudenberg, G. Getz, M. Meyerson, L. A. Mirny, *Nat. Biotechnol.* **29**, 1109–1113 (2011).
4. Y. Zhang *et al.*, *Cell* **148**, 908–921 (2012).
5. M. R. Hübner, D. L. Spector, *Annu. Rev. Biophys.* **39**, 471–489 (2010).
6. J. Dekker, K. Rippe, M. Dekker, N. Kleckner, *Science* **295**, 1306–1311 (2002).
7. E. Lieberman-Aiden *et al.*, *Science* **326**, 289–293 (2009).
8. Y. Markaki *et al.*, *Cold Spring Harb. Symp. Quant. Biol.* **75**, 475–492 (2010).
9. J. R. Dixon *et al.*, *Nature* **485**, 376–380 (2012).
10. E. P. Nora *et al.*, *Nature* **485**, 381–385 (2012).
11. A. Sanyal, B. R. Lajoie, G. Jain, J. Dekker, *Nature* **489**, 109–113 (2012).
12. W. Flemming, *Schriften des Naturwissenschaftlichen Vereins für Schleswig-Holstein* **3**, 23 (1878).
13. E. J. DuPraw, *Nature* **209**, 577–581 (1966).
14. A. L. Bak, J. Zeuthen, F. H. Crick, *Proc. Natl. Acad. Sci. U.S.A.* **74**, 1595–1599 (1977).
15. M. P. Marsden, U. K. Laemmli, *Cell* **17**, 849–858 (1979).
16. J. R. Swedlow, T. Hirano, *Mol. Cell* **11**, 557–569 (2003).
17. K. Maeshima, M. Eltsov, *J. Biochem.* **143**, 145–153 (2008).
18. J. R. Paulson, U. K. Laemmli, *Cell* **12**, 817–828 (1977).
19. K. Maeshima, U. K. Laemmli, *Dev. Cell* **4**, 467–480 (2003).
20. J. Sedat, L. Manuelidis, *Cold Spring Harb. Symp. Quant. Biol.* **42**, 331–350 (1978).
21. A. S. Belmont, J. W. Sedat, D. A. Agard, *J. Cell Biol.* **105**, 77–92 (1987).
22. Y. Nishino *et al.*, *EMBO J.* **31**, 1644–1653 (2012).
23. J. F. Marko, *Chromosome Res.* **16**, 469–497 (2008).
24. N. Kireeva, M. Lakonishok, I. Kireev, T. Hirano, A. S. Belmont, *J. Cell Biol.* **166**, 775–785 (2004).
25. J. Dostie *et al.*, *Genome Res.* **16**, 1299–1309 (2006).
26. M. Imakaev *et al.*, *Nat. Methods* **9**, 999–1003 (2012).
27. Materials and methods are available as supplementary materials on *Science* Online.
28. M. Simonis *et al.*, *Nat. Genet.* **38**, 1348–1354 (2006).
29. G. Fudenberg, L. A. Mirny, *Curr. Opin. Genet. Dev.* **22**, 115–124 (2012).
30. A. Rosa, N. B. Becker, R. Everaers, *Biophys. J.* **98**, 2410–2419 (2010).
31. R. Lua, A. L. Borovinskiy, A. Y. Grosberg, *Polymer (Guildf.)* **45**, 717–731 (2004).
32. G. Li, G. Sudlow, A. S. Belmont, *J. Cell Biol.* **140**, 975–989 (1998).
33. Y. G. Strukov, A. S. Belmont, *Biophys. J.* **96**, 1617–1628 (2009).
34. J. F. Marko, E. D. Siggia, *Mol. Biol. Cell* **8**, 2217–2231 (1997).
35. E. Fussner *et al.*, *EMBO Rep.* **13**, 992 (2012).
36. K. Maeshima, S. Hihara, H. Takata, *Cold Spring Harb. Symp. Quant. Biol.* **75**, 439–444 (2010).
37. Y. Adachi, M. Luke, U. K. Laemmli, *Cell* **64**, 137–148 (1991).
38. K. Samejima *et al.*, *J. Cell Biol.* **199**, 755–770 (2012).
39. J. L. Sikorav, G. Jannink, *Biophys. J.* **66**, 827–837 (1994).
40. D. A. Jackson, P. Dickinson, P. R. Cook, *EMBO J.* **9**, 567–571 (1990).
41. W. C. Earnshaw, U. K. Laemmli, *J. Cell Biol.* **96**, 84–93 (1983).
42. T. Hirota, D. Gerlich, B. Koch, J. Ellenberg, J. M. Peters, *J. Cell Sci.* **117**, 6435–6445 (2004).
43. E. Alipour, J. F. Marko, *Nucleic Acids Res.* **40**, 11202–11212 (2012).
44. N. Kleckner *et al.*, *Proc. Natl. Acad. Sci. U.S.A.* **101**, 12592–12597 (2004).
45. K. D. Sarge, O. K. Park-Sarge, *Trends Biochem. Sci.* **30**, 605–610 (2005).
46. W. Deng, G. A. Blobel, *Curr. Opin. Genet. Dev.* **20**, 548–554 (2010).
47. N. E. Follmer, A. H. Wani, N. J. Francis, *PLOS Genet.* **8**, e1003135 (2012).
48. S. Kadauke *et al.*, *Cell* **150**, 725–737 (2012).
49. Y. G. Strukov, Y. Wang, A. S. Belmont, *J. Cell Biol.* **162**, 23–35 (2003).
50. P. König, M. B. Braunfeld, J. W. Sedat, D. A. Agard, *Chromosoma* **116**, 349–372 (2007).
51. Y. Zhang, D. W. Heermann, *PLOS ONE* **6**, e29225 (2011).


**Acknowledgments:** All data will be made publicly available through the Gene Expression Omnibus. This work was supported by grants from the National Cancer Institute (Physical Sciences–Oncology Center at MIT U54CA143874 to L.A.M.) and the National Human Genome Research Institute (HG003143 to J.D.), the Human Frontier Science Program (to J.D.), and a W. M. Keck Foundation distinguished young scholar in medical research grant (to J.D.). We thank J. A. Stamatoyannopoulos and R. Humbert for designing part of the 5C primers; C. Smith and A. Hawkins for technical help; J. Benanti for providing HFF1 cell stock and discussion; M. Walhout, Dekker lab, and Mirny lab members for discussions; and the UMMS deep sequencing core for sequencing 5C and Hi-C libraries. The data are available at ArrayExpress database www.ebi.ac.uk/arrayexpress, accession no. E-MTAB-1948. Information about Gene Expression Omnibus accession nos. can be found in the supplementary materials. Data visualizations can also be found at http://hic.umassmed.edu and http://mirnylab.mit.edu.

### Supplementary Materials

www.sciencemag.org/content/342/6161/948/suppl/DC1
Materials and Methods
Figs. S1 to S26
Tables S1 to S3
References
Movies S1 to S6

4 February 2013; accepted 17 October 2013
Published online 7 November 2013;
10.1126/science.1236083

Editor's Summary

**Chromosome Conundrum**

The three-dimensional organization of chromosomal DNA within the cell nucleus plays an important role in gene regulation. **Naumova *et al.*** (p. 948, published online 7 November; see the Perspective by **Kleckner *et al.***) used chromosome conformation capture-based methods in human tissue culture cells to analyze the higher order folding of human chromosomes across the cell cycle. During interphase the chromosomes showed locus-specific compart-mentalization. In mitotic cells, on the other hand, the chromosome organization was more linear, consistent with arrays of consecutive chromatin loops.